Effect of the Hydrophilic Size on the Structural Phases of Aqueous Nonionic Gemini Surfactant Solutions

Mu-Ping Nieh,[†] Sanat K. Kumar,[‡] Raymond H. Fernando,[§] Ralph H. Colby,[||] and John Katsaras*,[†]

Neutron Program for Material Research, National Research Council, Chalk River Laboratory, Chalk River, Ontario, Canada K0J 1J0, Department of Chemical Engineering, Rensselaer Polytechnic Institute, Troy, New York 12210, Department of Chemistry and Biochemistry, California Polytechnic State University, San Luis Obispo, California 93407, and Department of Materials Science and Engineering, Pennsylvania State University, University Park, Pennsylvania 16802

Received February 27, 2004. In Final Form: August 3, 2004

Aggregate structures of aqueous nonionic Gemini surfactant solutions, α,α′-[2,4,7,9-tetramethyl-5-decyne-4,7-diyl]bis[ω-hydroxyl-polyoxyethylene] with three different length polyoxyethylenes (i.e., 10, 20, and 30 ethylene oxide monomers, denoted from now on as S-10, S-20, and S-30, respectively), are investigated using small angle neutron scattering, dynamic light scattering, and fluorescence spectroscopy. For S-10 at low surfactant concentrations (C_s < 0.9 wt %), large "clusters", with an average hydrodynamic radius $\langle R_H \rangle$ > 40 nm, are found to coexist with monomers. At intermediate C_s (0.9 < C_s < 2 wt %), some clusters break down forming micelles, with an $\langle R_H \rangle \sim 2-3$ nm, while the remaining clusters coexist with micelles. Increasing C_s further (>2 wt %) results in a pure micellar phase with little or no clusters present. S-20 and S-30 mixtures, on the other hand, differ from S-10 in that irrespective of surfactant concentration, large clusters and small monomers/dimers are found to coexist, while there is no direct evidence for the presence of micelles.

Introduction

Gemini surfactants are composed of two or more pairs of hydrophilic and hydrophobic groups connected to each other with a spacer.[1] Usually, their critical micellar concentration (cmc) in aqueous solutions is much lower than the cmc of conventional surfactants with the same hydrophilic and hydrophobic groups. As a result, smaller amounts of Gemini surfactants are needed to modify the surface tension of the solution.

In the past decade, many aqueous solutions of ionic Gemini surfactants[2−11] and their mixtures with other surfactants[12−17] have been investigated to understand the various parameters that affect their aggregate structures. Some of these parameters are hydrophobic tails asymmetry,[2−4] temperature, concentration,[5−7,12] tail hydrophobicity,[8,13] salt concentration,[9,15] properties of the spacers,[10,14−17] and the asymmetry of the counterpart surfactant.[11] These studies have shown that ionic Gemini surfactants composed of small hydrophilic headgroups and long hydrocarbon tails (>12 carbons) form a variety of structures (e.g., spherical, discoidal, threadlike micelles, vesicles, and lamellae).

Recently, nonionic Gemini surfactants have been synthesized.[18,19] However, morphological studies of these surfactants are rare. A recent transmission electron microscopy study reported that the phase behavior of nonionic glycosylated Gemini surfactants in aqueous solutions was strongly dependent on the rigidity and length of the spacers.[20] Menger and Mbadugha also reported on the rich structural behavior of nonionic Gemini surfactants having different tail lengths.[10] To our knowledge, the effect of the hydrophilic group's size on the resultant structure has not been systematically investigated.

The nonionic Gemini surfactants in our study, α,α′-[2,4,7,9-tetramethyl-5-decyne-4,7-diyl]bis[ω-hydroxyl-polyoxyethylene] (Figure 1) with $m + n$ ethylene oxide (EO) segments, are commonly used to lower the dynamic surface tension of solutions and as defoaming agents, metalwork lubricants, and pressure-sensitive adhesives. The molecules have two hydrophilic poly(ethylene oxide) (PEO)

[†] National Research Council.
[‡] Rensselaer Polytechnic Institute.
[§] California Polytechnic State University.
[||] Pennsylvania State University.

(1) Hait, S. K.; Moulik, S. P. *Curr. Sci.* **2002**, *82*, 1101−1111.
(2) Oda, R.; Huc, I.; Candau, S. J. *Chem. Commun.* **1997**, *21*, 2105−2106.
(3) Oda, R.; Huc, I.; Homo, J.-C.; Heinrich, B.; Schmutz, M.; Candau, S. *Langmuir* **1999**, *15*, 2384−2390.
(4) Sikirić, M.; Primožič, I.; Filipović-Vinceković, N.; Heinrich, B. *J. Colloid Interface Sci.* **2002**, *250*, 221−229.
(5) Aswal, V. K.; De, S.; Goyal, P. S.; Bhattacharya, S.; Heenan, R. K. *J. Chem. Soc., Faraday Trans.* **1998**, *94*, 2965−2967.
(6) Bernheim-Groswasser, A.; Zana, R.; Talmon, Y. *J. Phys. Chem. B* **2000**, *104*, 4005−4009.
(7) Oelschlaeger, Cl.; Waton, G.; Candau, S. J.; Cates, M. E. *Langmuir* **2002**, *18*, 7265−7271.
(8) Huc, I.; Oda, R. *Chem. Commun.* **1999**, *20*, 2025−2026.
(9) Knaebel, A.; Oda, R.; Mendes, E.; Candau, S. *Langmuir* **2000**, *16*, 2489−2494.
(10) Menger, F. M.; Mbadugha, B. N. A. *J. Am. Chem. Soc.* **2001**, *123*, 875−885.
(11) Menger, F. M.; Peresypkin, V. *J. Am. Chem. Soc.* **2001**, *123*, 5614−5615.
(12) Zana, R.; Lévy, H.; Kwetkat, K. *J. Colloid Interface Sci.* **1998**, *197*, 370−376.
(13) Oda, R.; Huc, I.; Danino, D.; Talmon, Y. *Langmuir* **2000**, *16*, 9759−9769.
(14) Bernheim-Groswasser, A.; Zana, R.; Talmon, Y. *J. Phys. Chem. B* **2000**, *104*, 12192−12201.
(15) Buhler, E.; Mendes, E.; Boltenhagen, P.; Munch, J. P.; Zana, R.; Candau, S. J. *Langmuir* **1997**, *13*, 3096−3102.
(16) Alargova, R. G.; Kochijashky, I. I.; Sierra, M. L.; Kwetkat, K. J.; Zana, R. *J. Colloid Interface Sci.* **2001**, *235*, 119−129.
(17) Danino, D.; Talmon, Y.; Zana, R. *J. Colloid Interface Sci.* **1997**, *185*, 84−93.
(18) Castro, M. J. L.; Kovenski, J.; Cirelli, A. F. *Tetrahedron* **1999**, *55*, 12711−12722.
(19) Bertho, J.-N.; Coué, A.; Ewing, D. F.; Goodby, J. W.; Letellier, P.; Mackenzie, G.; Plusquellec, D. *Carbohydr. Res.* **1997**, *300*, 341−346.
(20) Wathier, M.; Polidori, A.; Ruiz, K.; Fabiano, A.-S.; Pucci, B. *New J. Chem.* **2001**, *25*, 1588−1599.

10.1021/la0494831 CCC: $27.50
Published on Web 09/08/2004

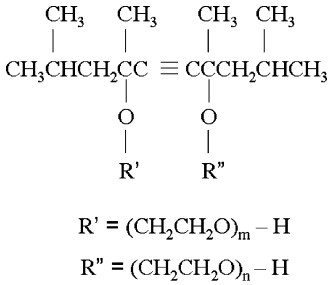

R' = $(CH_2CH_2O)_m - H$

R" = $(CH_2CH_2O)_n - H$

Figure 1. Chemical structure of α,α′-[2,4,7,9-tetramethyl-5-decyne-4,7-diyl]bis[ω-hydroxyl-polyoxyethylene].

chains connected to a 14-carbon hydrophobic "hub"; the segmental lengths (m and n) of these two PEO chains are not necessarily identical. In this paper, the surfactants will be named as follows: S-$m + n$, (e.g., S-10 has a total of 10 EO monomers per molecule, $m + n = 10$). More than a decade ago, Sato and Kishimoto first investigated aqueous S-10 solutions using vapor pressure depression, viscosity measurements,[21] enthalpy of micellation,[22] osmotic pressure,[23] and NMR spectroscopy.[24] They observed two cmc values (0.9 and 2 wt %) but could not conclusively ascribe a morphology to either of these two transitions. Nevertheless, Sato and Kishimoto assumed the presence of monomers (below the first cmc) and micelles (beyond the first and second cmc's) even though the monomer morphology was inconsistent with their viscosity data.[21]

Using small angle neutron scattering (SANS), dynamic light scattering (DLS), and fluorescence spectroscopy (FS), the present study reports on the structural phases of aqueous S-10, S-20, and S-30 solutions. Specifically, the effect of the hydrophilic group's size on the aggregate structure is thoroughly investigated. We have found that, as a function of increasing surfactant concentration, an unusual structural phase transition takes place, that is, large clusters → micelles, which to the best of our knowledge has not been previously observed in other single-component surfactant systems and possibly explains Sato and Kishimoto's viscosity data.[21] In addition, concentration- and time-dependent studies are conducted to understand the formation and stability of the aggregate structures.

Experimental Methods

Sample Preparation. S-10, S-20, and S-30 surfactants were obtained from Air Products & Chemicals, Inc., and used without further purification. S-10 and S-20 have the consistency of a viscous fluid (S-10 is transparent, while S-20 has a brown color), while S-30 is a brown gel. All three surfactants are solvated using water. For SANS measurements, D_2O instead of H_2O was used (99%, Cambridge Isotope, Inc.) to better contrast the surfactant from the solvent. The surfactant concentration, C_s, was varied from 0.2 to 5 wt %. For DLS measurements, samples were dissolved in distilled deionized H_2O, which was filtered (pore size = 100 nm) prior to mixing with the surfactants. Surfactant concentrations between 0.2 and 3 wt % were used to prevent the possibility of strong interparticle interactions, thus, allowing us to use the Stokes−Einstein equation in calculating the hydrodynamic radius (R_H). In the case of FS experiments, pyrene (Py; Sigma Chemical Co.) was predissolved in distilled deionized water at a concentration of 2 ppm and then mixed with the surfactants to obtain the desired concentrations. All measurements, irrespective of the technique used, were carried out at room temperature (~23 °C).

Technique and Data Reduction. *SANS.* Experiments were performed using the 30m NG7 SANS instrument located at the National Institute of Standards and Technology (Gaithersburg, MD). The 6-Å wavelength neutrons were detected using a two-dimensional (2-D) detector with a 20-cm offset. Two sample-to-detector distances (SDD) were employed (SDD = 1.5 and 14 m), covering a q range between 0.004 and 0.3 $Å^{-1}$. The scattering vector, q, is defined as $(4\pi/\lambda)\sin(\theta/2)$, where θ is the scattering angle and λ is the wavelength.

Samples were placed in circular quartz cells with path lengths varying from 2 to 4 mm, depending on the scattered intensity. The 2-D raw data were corrected for both ambient background and empty cell scattering and then put on an absolute scale (cross section per unit volume) through a procedure that estimates the neutron flux impinging on the sample.[25] The data were then circularly averaged to yield the one-dimensional intensity profile, $I(q)$. The incoherent scattering was approximated from the high-q intensity plateau data for each sample and then subtracted from the corresponding reduced data. The corrected $I(q)$ is, thus, proportional to the product of the form factor, $P(q)$, which accounts for the morphology of the aggregates, and the structure factor, $S(q)$, which describes the interaggregate interactions. In our case, because only dilute samples were studied, only $P(q)$ is of consequence [i.e., $I(q) \sim P(q)$].

DLS. The Stokes−Einstein formula [eq 1] is commonly used to describe the relationship between the diffusion coefficient D and the hydrodynamic radius R_H of dilute, neutral monodisperse spherical particles in solution and can be written as follows:

$$D = \frac{kT}{6\pi\eta_w R_H} \tag{1}$$

where k, T, and η_w are the Boltzmann constant, the absolute temperature, and the viscosity of water, respectively. For particles of different shapes (e.g., disk, cylinder, etc.), R_H represents an equivalent hydrodynamic radius. For DLS measurements, the intensity time correlation function, $G(\tau)$, is defined as follows:

$$G(\tau) = \int_0^\infty I(t)\, I(t+\tau)\, \mathrm{d}t \tag{2}$$

where τ is the delay time. From the Siegert relation, $G(\tau)$ can be expressed in terms of the field autocorrelation function, $g(\tau)$, as

$$G(\tau) = 1 + \gamma g(\tau)^2 \tag{3}$$

where γ is the instrument-dependent coherence factor. For a polydisperse system, $g(\tau)$ is the sum of the exponential decays contributed from all particles and for a specific delay time, τ, and can be written as

$$g(\tau) = \sum_i A_i e^{-D_i q^2 \tau} \tag{4}$$

where q is the scattering vector and A_i represents the amplitude of the ith particle with diffusion coefficient D_i. Using eq 1, one can relate D_i to the corresponding hydrodynamic radius R_{Hi}.

CONTIN is used in analyzing the DLS data solving for a group of $g(\tau)$ through eigenvalue decomposition in combination with regularization, a smoothing technique used to overcome the ill-posed nature of a Laplace transform inversion. The size distribution function expressed in terms of intensity can, thus, be resolved as a function of D_i (or R_{Hi}). $\langle R_H \rangle$ is, thus, obtained using intensity as a weighting factor.

DLS experiments were conducted using a DynaPro/MS-X (Proteinsolutions, Inc.) light scattering setup, which measures the scattered intensity at a fixed scattering angle (θ) of 90°. The correlator has 256 channels with delay times between 1 and 10^5 μs. The instrument is equipped with a power-adjustable laser source ($\lambda = 782.8$ nm) and a temperature-controlled sample cell. The intensity overflow limit for the detector is $\sim 7 \times 10^6$ counts/s. The normalized intensity correlation function, $\bar{G}(\tau)$, was obtained by averaging over a given acquisition time (~10 s in our case). Prior to experimentation, the instrument was calibrated using standard polystyrene microbead aqueous solutions with particle sizes ranging between 1 nm and 1 μm ± 2%. DLS measurements

(21) Sato, S.; Kishimoto, H. *Bull. Chem. Soc. Jpn.* **1985**, *58*, 282−287.
(22) Sato, S.; Kishimoto, H. *J. Colloid Interface Sci.* **1988**, *123*, 216−223.
(23) Sato, S.; Kishimoto, H. *J. Colloid Interface Sci.* **1988**, *126*, 108−113.
(24) Sato, S. *J. Phys. Chem.* **1989**, *93*, 4829−4833.
(25) Glinka, C. J.; Barker, J. G.; Hammouda, B.; Krueger, S.; Moyer, J. J.; Orts, W. J. *J. Appl. Crystallogr.* **1998**, *31*, 430−445.

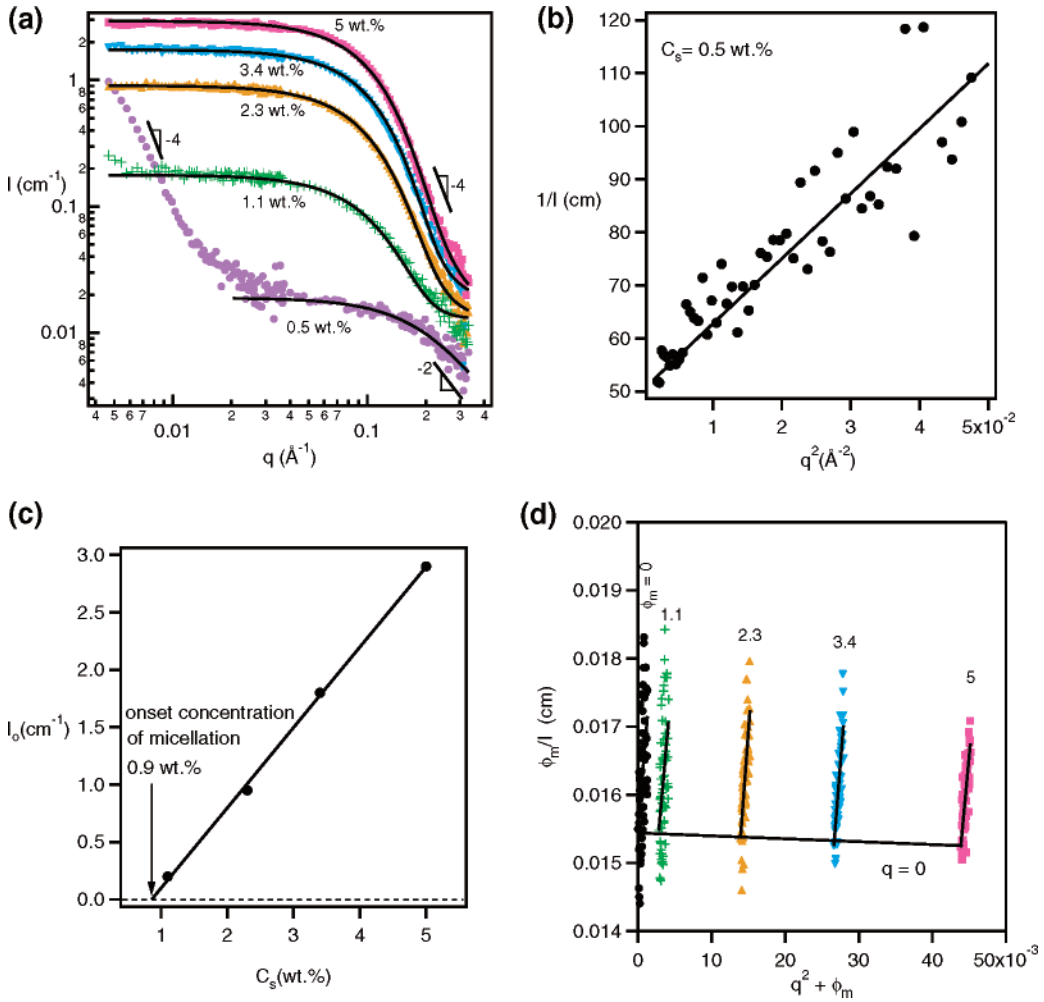

Figure 2. (a) SANS data of aqueous S-10 solutions ($0.5 \leq C_s \leq 5$ wt %). The solid lines are the best fit using the Debye relationship [eq 5] for the $C_s = 0.5$ wt % sample and a polydisperse spherical model with a hard sphere structure factor for the samples $1.1 \leq C_s \leq 5$ wt %. (b) $1/I$ versus q^2 plot constructed from the SANS data of the $C_s = 0.5$ wt % samples using a q range between 0.04 and 0.2 Å^{-1}. The slope from the plot is 1225 cm·Å^{-2}. (c) The intensity plateau, I_0, as a function of C_s for S-10 samples with $1.1 \leq C_s \leq 5$ wt %. The intercept, C_{s0}, is in agreement with the first cmc (e.g., 0.9 wt %) value, reported by Sato and Kishimoto.[21] (d) Zimm plots constructed from SANS data using the $1.1 \leq C_s \leq 5$ wt % samples and intensity data from the q range between 0.008 and 0.1 Å^{-1}.

were also taken at various time intervals after preparation, to investigate the time dependence of the surfactant systems.

FS. The SPEX Fluorolog 3 fluorimeter (Analytical Chemistry Division, NIST) has a double monochromator for selecting both the excitation and emission wavelengths. The excitation source is a 450-W Xe lamp. The emission intensity is measured using a Hamamatsu R928 photon counting photomultiplier tube and was collected at an angle of 90° from the incident excitation light. The λ of the excitation beam is 335 nm, and the detected wavelength of the emission beam ranged from 360 to 460 nm.

Py was used as the fluorescent probe and was predissovled in the solvent (H_2O) at a concentration of 2×10^{-6} g Py/g total. The surfactants were then prepared to the desired C_s using the Py-doped H_2O. The emission spectrum of Py contains five peaks in the range of 360−400 nm. The intensity ratio of the first peak (I_1) to the third peak (I_3), I_1/I_3, varies when the polarity of its surroundings changes.[26]

Results

S-10—Phase Behavior. Figure 2a shows SANS data for S-10 samples with C_s between 0.5 and 5 wt %. The scattering pattern of the 0.5 wt % sample is very different from those of the other samples, indicating that a structural phase transition occurs at $0.5 < C_s < 1.1$ wt %. This result is consistent with the first cmc (0.9 wt %) reported by Sato and Kishimoto;[21,23,24] however, the q^{-4} dependence of the scattered intensity at low-q values (up to $q \sim 0.02$ Å^{-1}) for the 0.5 wt % sample indicates the existence of structures exceeding 50 nm (e.g., "clusters"). This morphology is different than the expected monomers that one usually finds in surfactant solutions at concentrations below the cmc. Beyond the q^{-4} region, the scatted intensity plateaus ($0.03 < q < 0.1$ Å^{-1}) and exhibits a q^{-2} behavior indicative of small particles of size $\sim$ 1 nm. Because the intensity contribution from large structures, such as clusters, is mainly in the low-q regime and close to the probing limit of our instrument, it is not possible for us to obtain detailed structural information from the present data. Nevertheless, it is reasonable to assume that, for $q > 0.03$ Å^{-1}, the major contribution to the scattered intensity is from small particles whose size can be precisely obtained from SANS data. For this case, two methods are used to evaluate the size of the small particles, assuming that for the 0.5 wt % sample interparticle interactions are negligible.

The Debye function is commonly employed in describing the scattering curve of dilute polymer solutions and can be written as follows:

$$I(q) = \phi_{s,n}\Delta\rho^2 v_s n_s f(R_G{}^2 q^2) \qquad (5)$$

(26) Dong, D. C.; Winnik, M. A. *Can. J. Chem.* **1984**, *62*, 2560−2565.

Table 1. Best Fit Results of the Various Analyses Used for the Presence of Small Aggregates in S-10, S-20, and S-30 Solutions[a–c]

	S-10					S-20					S-30				
	C_s (wt %)														
	0.5	1.1	2.3	3.4	5	0.2	0.5	1	2.5	4	0.2	0.5	1	2.5	5
	Debye Fit														
C_m (wt %)	0.48					0.15	0.5	0.86	2.47	3.97	0.2	0.45	0.82	2.48	4.94
R_G (Å)	7.8					13.6	12.2	12.9	13.2	15.1	13.5	12.9	12.8	14.2	13.1
n_s	1					1.6	1.8	1.5	1.6	3	1.2	1.2	1.1	1.2	0.8
	Zimm Plot or $1/(I - q^2)$ Plot														
R_G (Å)	8.4	14.7 ± 3.5	14.7 ± 3.5	14.7 ± 3.5	14.7 ± 3.5	13.3 ± 2.1	13.3 ± 2.1	13.3 ± 2.1	13.3 ± 2.1		13.5 ± 1.2	13.5 ± 1.2	13.5 ± 1.2	13.5 ± 1.2	
n_s	1	17.2 ± 0.2	17.2 ± 0.2	17.2 ± 0.2	17.2 ± 0.2	1.6 ± 0.2	1.6 ± 0.2	1.6 ± 0.2	1.6 ± 0.2		1.16 ± 0.14	1.16 ± 0.14	1.16 ± 0.14	1.16 ± 0.14	
	Polydisperse Sphere Model[d]														
R (Å)		14.1	14.3	15.3	14.3										

[a] Empty cells represent that the analysis is not available. [b] The contrast factor $\Delta\rho$ is calculated to be 5.92×10^{10}, 5.89×10^{10}, and 5.76×10^{10} cm^{-2} for S645, S480, and S485, respectively. [c] Molecular volumes v_s for S465, S480, and S485 are 1.06×10^{-21}, 1.53×10^{-21}, and 2.14×10^{-21} cm^3, respectively. [d] Using the spherical model to fit the polydispersity of S-10 samples yields a value ~0.28 ± 0.02. With the exception of sample S-10 $C_s = 0.5$ wt %, R_G and n_s values are obtained from Zimm plots by extrapolating to $C_s = 0$.

where $f(x) = (2/x^2)(e^{-x} - 1 + x)$; $\phi_{s,n}$ is the volume fraction of the surfactant aggregates; $\Delta\rho$ is the scattering length density difference, or so-called contrast factor between the surfactant and D_2O (~5.92×10^{10} cm^{-2} for S-10); v_s is the molecular volume of the surfactant (1.06×10^{-21} cm^3 for S-10); n_s is the number of aggregation particles; and R_G is average radius of gyration. In the range of $q > 0.04$ Å^{-1} the data are fitted using the Debye function [solid line in Figure 2a], and an R_G of ~7.8 ± 1.0 Å is obtained.

A more general approach for determining the R_G of large aggregates (i.e., $R_G q < 1$) from SANS data is

$$\frac{\phi_{s,n}}{I(q)} = \frac{1}{\Delta\rho^2[1 - (R_G^2/3)q^2 + ...)}\left(\frac{1}{v_s n_s} + 2A_2\phi_{s,n} + ...\right) \quad (6)$$

where A_2 is the second virial coefficient related to the interparticle interaction, whose sign indicates the net interaction between aggregates (+ = repulsive, − = attractive). By plotting $\phi_{s,n}/I(q)$ versus q^2, a straight line is obtained in the regime where $R_G q < 1$, corresponding to a q range of $0.04 < q < 0.2$ Å^{-1}. Assuming that interparticle interactions are negligible for this dilute sample (i.e., $A_2 \sim 0$), the slope of the fitted line is then proportional to $[1/(\Delta\rho^2 v_s n_s)](R_G^2/3)$. The resultant R_G value of 8.3 ± 1.0 Å from the graph shown in Figure 2b is consistent with the R_G obtained from our previous fit using the Debye function.

Kinugasa et al. reported experimental data on the relationship between M_W (molecular weight) and R_G for PEO in water.[27]

$$\langle R_G^2 \rangle = 4.08 \times 10^{-18} \times M_W^{1.1} \quad (7)$$

Because the major component of S-10 is PEO and there is no predicted or experimental value for R_G of S-10, we can roughly estimate its value, using eq 7. It turns out that R_G for S-10 is 7.2 Å/monomer and is in good agreement with the value obtained from the Debye fit [Figure 2a] and the fit to the plot in Figure 2b. It, therefore, seems that the small particles coexisting with clusters in solution are monomers.

Using the Debye function, the best fit result of $\phi_{s,n}$ for $n_s = 1$ is 0.0051, which translates into 0.48 wt %. This means that >95% of the 0.5 wt % S-10 sample is comprised of monomers, although the few clusters that do exist contribute, because of their size, strongly to the scattered intensity at low q.

For $C_s \geq 1.1$ wt %, the strong scattering intensity at low q vanishes [Figure 2a], indicating the absence of clusters. All SANS curves are characterized by an intensity plateau, I_0, at low q followed by a monotonic decay at higher q, typical of scattering from micelles. Given the fact that in the high-q regime the scattered intensity decays as q^{-4}, instead of q^{-2} [Figure 2a], the Debye function [eq 5] cannot be applied to fit these data. Because I_0 is proportional to the micellar number density, one can obtain the onset concentration for micellation, C_{s0} (~0.9 wt %), from $I_0 = 0$, as shown in Figure 2c. This result is consistent with the previously reported cmc.[21,23,24] Therefore, the micelle concentration can be obtained from the expression $C_s - C_{s0}$, while R_G, n_s, and A_2 (related to the interparticle interaction) of the micelles can be obtained from a Zimm plot of ϕ_m/I versus $(q^2 + b\phi_m)$. ϕ_m is the volume fraction of micelles and is equivalent $(C_s - C_{s0})$, where b is a multiplier used to separate the various ϕ_m data for better visualization.

Figure 2d shows Zimm plots for four S-10 sample concentrations (1.1 and 5 wt %) obtained from SANS data in the q range of between 0.01 and 0.04 Å^{-1}. The lower q limit is determined from the deviation of the plateau resulting from large clusters, while the higher q limit is chosen so that $qR_G < 1$. The slopes of the extrapolated lines at $\phi_m = 0$ and $q = 0$ are $[1/(\Delta\rho^2 v_s n_s)](R_G^2/3)$ and $2A_2/(\Delta\rho^2 b)$, respectively, and their intercepts yield, from eq 6, $1/(\Delta\rho^2 v_s n_s)$. The values for R_G, n_s, and A_2 obtained from the Zimm plots are 14.7 ± 3.5 Å, 17.2 ± 0.2, and $(-2 \pm 6) \times 10^{-5}$ mol/cm^3 and are summarized in Table 1. The aggregation number, n_s, for micelles is comparable to values reported in the literature.[21–23] Because the error for A_2 is comparable to its experimental value, the sign of A_2 cannot be determined from the present result. However, the interparticle interaction, if any, is weak.

The data are also fitted using a model of polydisperse spheres in combination with a hard sphere structure factor (to a first order approximation), where only ϕ_m, the sphere's radius, and the polydispersity are allowed to vary. The best fit result (Table 1) yields an R comparable to R_G and a polydispersity $\Delta R/\langle R \rangle$ (ΔR is the standard deviation of R and $\langle R \rangle$ is the mean value of R) of ~0.28 ± 0.02.

DLS results for various C_s S-10 samples equilibrated over 1 week are in agreement with the SANS data and provide further detailed information about the various morphologies (Figure 3). A single population of clusters

(27) Kinugasa, S.; Nakahara, H.; Fudagawa, N.; Koga, Y. *Macromolecules* **1994**, *27*, 6889−6892.

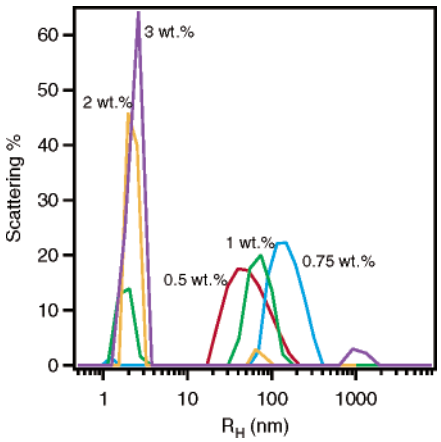

Figure 3. Size distribution functions from DLS measurements of S-10 samples with $C_s = 0.5$, 0.75, 1.0, 2.0, and 3.0 wt %. The data were taken at least 1 week after equilibration.

with an $\langle R_H \rangle \sim 40$ nm is observed for the 0.5 wt % S-10 solution (Figure 3). As a result of inadequate instrumental resolution, S-10 monomers are too small to be seen. However, as C_s increases to 0.75 wt %, the cluster $\langle R_H \rangle$ grows to >100 nm, while a small population of aggregates with an $\langle R_H \rangle \sim 1.3$ nm is also observed. A dramatic change in the size distribution function is observed as C_s is further increased to 1 wt %. At this wt %, two $\langle R_H \rangle$ populations appear, one with a value between 1.8 and 2.3 nm and another with $\langle R_H \rangle \sim 100$ nm, a good indication of micelle and cluster coexistence. As C_s is increased to ≥2 wt %, most of the clusters disappear, and $\langle R_H \rangle$ is found centered ~2.3 nm. This phase transition is consistent with the second cmc (2 wt %) reported by Sato and Kishimoto.[21] It is reasonable to assume that, for micelles, $\langle R_H \rangle$ will be slightly larger than R_G for the following reasons: (a) R_G is defined as the second moment average length from each point of the object to the mass center, while $\langle R_H \rangle$ is related to the hydrodynamic behavior of the particles. In the case of a sphere with radius R, R_G is equal to $(3/5)^{1/2}R$, but $\langle R_H \rangle = R$. (b) The measured $\langle R_H \rangle$ includes H_2O molecules incorporated with the hydrophilic EO groups, while R_G, obtained from Zimm plots, is based on the contrast between the D_2O and the surfactant molecules and does not account for the volume of associated D_2O. (c) The $\langle R_H \rangle$ is normalized using the scattered intensity (volume^2), instead of the volume, as is the case for $\langle R_G \rangle$. As a result, a higher $\langle R_H \rangle$ value for particles of the same size distribution function is obtained.

From SANS and DLS data of S-10 solutions, we conclude that a sharp transition takes place at $C_s \sim 0.9$ wt % where micelles first form in a dilute solution of large clusters. These clusters already exist at $C_s < 0.9$ wt %. For $C_s >$ 2 wt %, micelles predominate, while coexisting clusters are few in number or nonexistent.

Fluorescent spectroscopy using Py molecules as probes was employed to investigate the detailed structure of the clusters. Because Py molecules prefer to remain in a hydrophobic environment and the first-to-third peak intensity ratio (I_1/I_3) is sensitive to the environment of Py molecules, the location of Py molecules in solution can be deduced. Figure 4a shows the emission spectra of Py-doped pure water and S-10 samples at concentrations ≤1 wt %. Figure 4c depicts the relationship of I_1/I_3 as a function of C_s. For a pure water/Py solution, the I_1/I_3 ratio was found to be 1.78 ± 0.08, similar to the 1.87 value reported in the literature.[26] As C_s increases, the ratio remains unaltered until ~0.8 wt %, the approximate value of the first cmc, where it suddenly drops. This indicates that most Py molecules are no longer in water but instead go into the hydrophobic region of micelles [Figure 4c]. Two possibilities may explain the high I_1/I_3 values in the case of clusters (i.e., Py existing in the water phase). First, the fact that the cluster population density is low means that only a small fraction of Py molecules can reside in the cluster's hydrophobic region. Second, the cluster hydrophobic region may not be large enough to accommodate the Py molecules, so they remain in water.

S-10—Time Dependence. The stability of S-10 clusters and micelles is also investigated as a function of time after sample preparation. Figure 5a shows the size distribution functions for S-10 clusters at $C_s = 0.75$ wt % over a period of 26 days. Although, in some cases (1 h and 11 days), micelles are also observed, here we will focus on the size evolution of clusters. At $C_s = 0.75$ wt %, S-10 clusters have an initial R_H value of 50 nm, which increases over time to ~170 nm. Figure 5b illustrates that clusters reach their equilibrium R_H value after ~100 h. A similar trend is observed for 0.5 wt % sample clusters. The final cluster size is C_s-dependent (higher C_s results in larger clusters) as shown in Figure 5b. Continuous growth of surfactant aggregates over a period of several months was previously observed in some conventional ionic surfactant mixtures which yielded unilamellar vesicles (ULVs).[28,29] This growth was attributed to the slow process of vesicular formation, the limiting factor being the partitioning of surfactant molecules between inner and outer leaflets of the bilayer making up the ULV.[29]

The same time-dependent study was carried out using a 1 wt % mixture (Figure 6). Clusters are not observed until 1 h after sample preparation. After 20 min there is a broad micellar size distribution, which decreases with time. After 1 h the micelles reach a size distribution that remains practically unaltered over a period of 13 days. As for the clusters, not only does their population increase with time but their size also grows continuously, in the same manner as that of the low C_s samples, indicating that some micelles transform into clusters. Moreover, SANS data of 1 wt % samples 3 h and 17 days after preparation (data not shown) are virtually identical, the exception being the very low-q regime ($q < 0.004$ Å^{-1}) where the intensity of the 17-day sample is higher, indicating that the clusters are growing both in size and in number. For the $C_s \geq 2$ wt % samples the micelles are stable over a period of 2 weeks. Occasionally clusters are found in small populations (data not shown).

S-20 and S-30—Phase Behavior. S-20 and S-30 samples yielded, at corresponding C_s values, SANS patterns [Figure 7a,b] resembling those of 0.5 wt % S-10 samples, indicating that similar structures are present in all three mixtures. As a function of q, the scattering pattern is characterized by a monotonic decay, followed by a plateau region, and then another decay, again implying the coexistence of clusters and small particles. For the $C_s \leq 2.5$ wt % sample, the intensity decay at $q > 0.1$ Å^{-1} follows a q^{-2} dependence indicating that the Debye relationship [eq 5] is appropriate in describing the data. The plateau intensity, I_0, is determined by fitting the data in the regime of $q > 0.04$ Å^{-1}. Plotting I_0 versus C_s yields a straight line and the onset concentration, C_{s0}, for small particles [insets to Figure 7a,b]. However, unlike S-10 solutions, C_{s0} is practically 0, indicating that either micelles are not forming or the cmc is extremely small in these two systems. Zimm plots (Figure 8) of these two systems were constructed with the $C_s \leq 2.5$ wt % samples

(28) Verbrugghe, S.; Laukkanen, A.; Aseyev, V.; Tenhu, H.; Winnik, F. M.; Prez, F. E. D. *Polymer* **2003**, *44*, 6807−6814.
(29) Iampietro, D. J.; Kaler, E. W. *Langmuir* **1999**, *15*, 8590−8601.

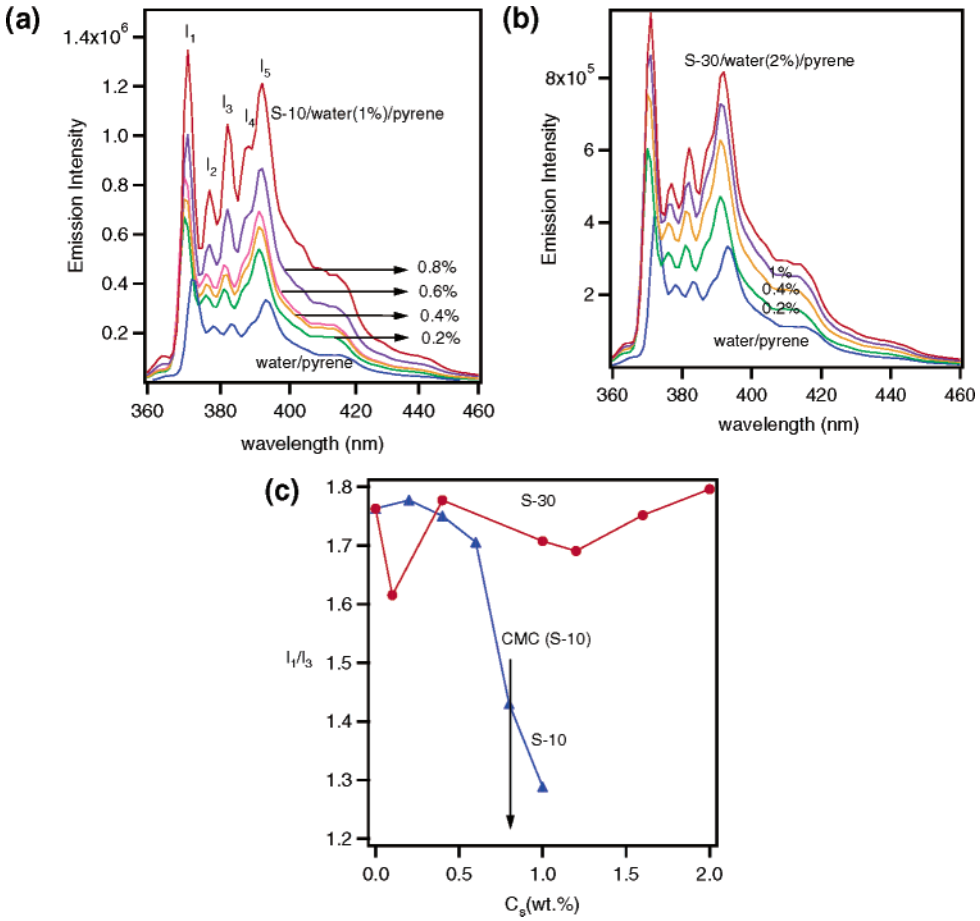

Figure 4. Fluorescent emission spectra for (a) S-10/water/Py systems with C_s varying from between 0 and 1 wt % and (b) S-30/water/Py systems with C_s varying from between 0 and 2 wt %. (c) The ratios of I_1/I_3 are plotted as a function of C_s for the data sets in parts a and b. A sharp transition for the S-10 samples is observed at ~0.8 wt %.

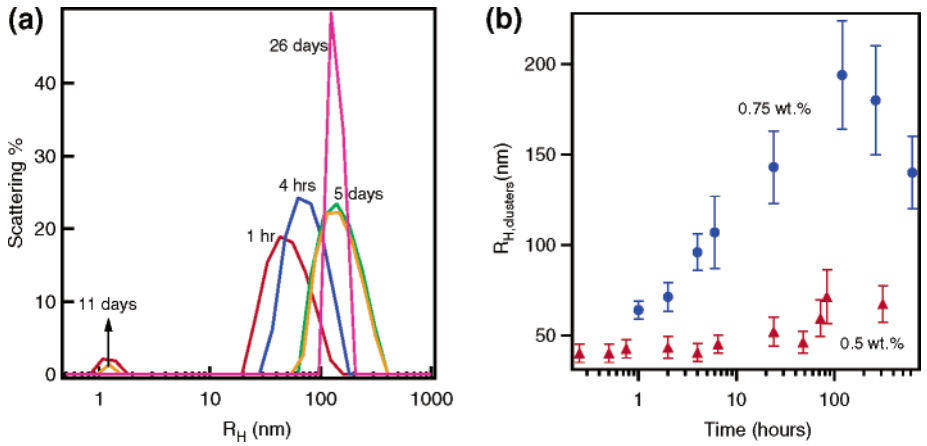

Figure 5. (a) Size distribution function from DLS time-dependent studies of a 0.75 wt % S-10 solution. The peak corresponding to the cluster morphology continuously shifts, with time, to a larger size distribution. (b) The evolution of S-10 clusters, with time, at two different C_s values (e.g., 0.75 and 0.5 wt %).

in the same manner as discussed previously. For S-20, R_G and n_s are found to be 13.3 ± 2.1 Å and 1.6 ± 0.2, respectively, and representative of dimers. On the other hand, the obtained R_G and n_s values of S-30 solutions are 13.5 ± 1.2 Å and 1.2 ± 0.14, respectively, indicating the predominance of monomers. The A_2 value for S-20 is (2.2 ± 6.4) × 10^{-4} mol/cm^3. Again as in the case for S-10, the experimental error is comparable to the obtained value signifying weak interparticle interactions. The same can be said for the S-30 sample [A_2 = (2.6 ± 1.4) × 10^{-3} mol/cm^3]. R_G values from the Debye fits are similar to those obtained from the Zimm plots (Table 1).

For the C_s > 2.5 wt % samples, I_0 deviates from the fit for both S-20 and S-30 solutions [insets of Figure 7a,b]. On the other hand, the Debye relationship yields reasonable fits [Figure 7a,b]. In the case of S-20, the positive deviation of I_0 for the 4 wt % sample is possibly due to an increase of n_s, which is found to be ~3 from the Debye fit instead of 2 obtained from lower concentration samples. For S-30, the negative deviation of I_0 for the 5 wt % sample is most likely a structure factor effect arising from strong interparticle interactions.

The DLS data of S-20 solutions show a multimodal size distribution (data not shown). As a result, fluorescent

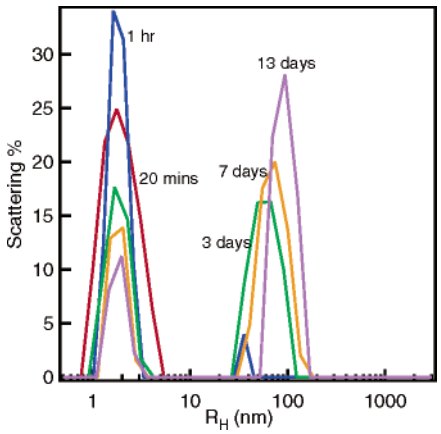

Figure 6. Size distribution function from DLS as a function of time for a 1.0 wt % S-10 solution. It is clear that both the size and the population density of clusters increase with time.

spectroscopy experiments were performed on S-30 samples with differing C_s [Figure 4b]. Unlike the S-10 system, the intensity ratio of I_1/I_3 remains constant at 1.7 ± 0.1 throughout a range of concentrations ≤2 wt % [Figure 4c], lending support to our conclusions derived from SANS data that the small particles found in S-30 solutions are monomers and not micelles.

Discussion

Clusters. Clusters are found in S-10 solutions with C_s < 2 wt % and all of the S-20 and S-30 solutions, regardless of C_s. The rheological behavior of S-10 solutions containing such clusters has been previously reported.[21] Moreover, the reduced viscosity exhibited by samples below 0.9 wt % was found to be ∼4, higher than the theoretical value of 2.5.[21] The previous interpretation by Sato and Kishimoto was that the highly hydrophilic EO groups contributed to the increase in the apparent volume fraction of the solute.[21] In fact, the unexpected high value of the reduced viscosity may be due to the presence of such clusters. Of note is that large cluster formation has been observed in some low C_s PEO-grafted polymers and disappeared at higher C_s in the same manner as S-10 solutions.[28] Although we do not present a detailed structure of the cluster morphology, judging by the slow kinetics in reaching an equilibrium phase,[29,30] it is likely that the clusters resemble a vesicular structure, consistent with the viscosity exhibited by this phase. Because the two EO branches of S-10 molecules are most likely not of equal length, the flip-flop of S-10 molecules taking place to minimize the curvature free energy results in a continuous size evolution and is consistent with the explanation given by Yatcilla et al.[30] The system, however, does not necessarily form bilayers because the trans configuration of the two EO branches, with respect to the triple bond, presumably results in a lower steric energy. Such a planar structure formed by the trans configuration of the two EO branches also rationalizes the possible insufficient hydrophobic volume needed for accommodating the Py molecules. Moreover, vesicular structures (e.g., unilamellar or multilamellar) were also found in other Gemini surfactants solutions.[11,13,14,17]

Another possible cluster morphology could be "microbubbles". They have recently been observed in water and can be removed via centrifugation.[31] SANS data from a degassed S-10 solution (∼0.7 wt %) continues to exhibit strong low-q intensity (data not shown), further solidifying the notion of clusters. Another possibility is that the surfactant molecules stabilize the microbubbles in solution. However, presently there is no experimental evidence supporting this assumption, except that these surfactants are commonly used for defoaming agents and the "stabilized" microbubbles might be able to prevent the formation of the larger bubbles that could lead to foaming.

The manner in which the scattered intensity decays as a function of q provides us with evidence of the gross morphologies present in various sample mixtures. For example, a q^{-4} dependence is indicative of spherical or nearly spherical objects or scattering media with a sharp interfacial boundary (two-phase coexistence). On the other hand, a q^{-1} describes rodlike particles, while extended sheets and random walk coils are characterized by a q^{-2} dependence. In Figure 7 the intensity decay, as exhibited by several samples ($C_s \leq 1$ wt % for both S-20 and S-30 solutions), does not follow a q^{-4} dependence. This may be ascribed to one of three possibilities or any combination of these. First, the structure of the above-mentioned clusters is far from isotropic (e.g., nonspherical). This argues against the possibility of "microbubbles", whose shape is most probably spherical. Another possibility could be that there is an insufficient amount of separation between the various contributions from the different morphologies in a mixture that the expected q^{-4} decay from the clusters could be buried in the signal arising from smaller particles. Finally, the continuous evolution of the clusters over the period of time it takes to collect the SANS data could result in a variable low-q slope.

Effect of the Size of the Hydrophilic Groups. Comparing the experimental results from the different surfactant samples, the size of the hydrophilic group is found to strongly affect the structural phase behavior. A cmc of ∼0.9 wt % was observed for S-10 solutions with an $n_s \sim 17.3$, while the n_s and R_G values of S-20 samples indicate the formation of dimers. S-30 with very long PEO chains form monomers as a result of the PEO branches being long enough to shield the hydrocarbon chains. The micellation of S-30 would result in a higher free energy than that of monomers due to a reduction in entropy. As a result, a trend of forming smaller micelles at a higher cmc is found as the hydrophilic groups become larger. This is also expected of surfactants with increased spontaneous curvature as a result of large-sized hydrophilic groups.[32]

Cluster → Micelle. The cluster → micelle transition as a function of increasing C_s is only clearly observed in S-10 solutions. This transition has previously been observed in some surfactant mixtures,[33−37] but to the best of our knowledge, not in single surfactant systems. Compared to micelles, clusters are much larger structures having a lower entropy. In addition, they are more stable at smaller C_s (<0.9 wt %), indicating a lower enthalpy. Therefore, the cluster → micelle transition can presumably be attributed to a decrease in the total free energy of the system by increasing the entropy. In the case of S-20 or S-30, the cluster → dimer or monomer transition is not

(30) Yatcilla, M. T.; Herrington, K. T.; Brasher, L. L.; Kaler, E. W.; Chiruvolu, S.; Zasadzinski, J. A. *J. Phys. Chem.* **1996**, *100*, 5874−5879.
(31) Glinka, C. (NCNR, NIST). Personal communication.
(32) Israelachvili, J. *Intermolecular and Surface Forces*, 2nd ed.; Academic Press: New York, 2000.
(33) Schurtenberger, P.; Mazer, N.; Waldvogel, S.; Känzig, W. *Biochim. Biophys. Acta* **1984**, *775*, 111−114.
(34) Caria, A.; Khan, A. *Langmuir* **1996**, *12*, 6282−6290.
(35) Marques, E. F.; Regev, O.; Khan, A.; da Graca Miguel, M.; Lindman, B. *J. Phys. Chem. B* **1998**, *102*, 6746−6758.
(36) Villeneuve, M.; Kaneshina, S.; Imae, T.; Aratono, M. *Langmuir* **1999**, *15*, 2029−2036.
(37) Egelhaaf, S. U.; Schurtenberger, P. *Phys. Rev. Lett.* **1999**, *82*, 2804−2807.

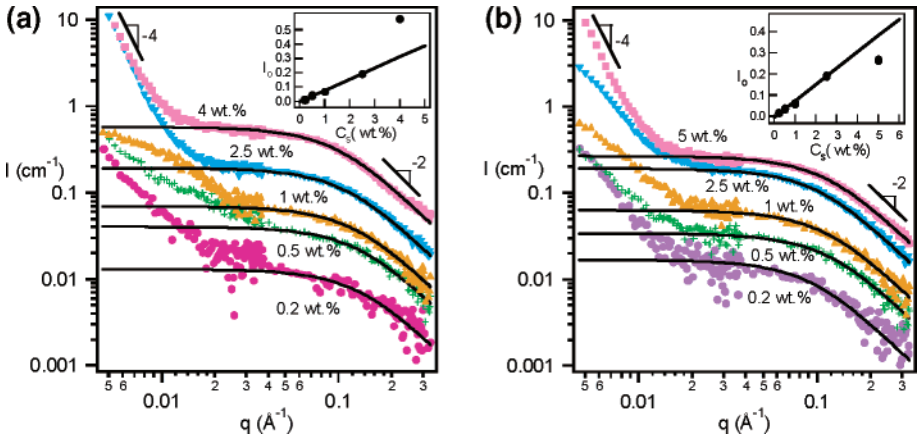

Figure 7. SANS results of (a) S-20 solutions ($0.2 \leq C_s \leq 4$ wt %) and (b) S-30 solutions ($0.2 \leq C_s \leq 5$ wt %). The solid curves are the Debye fits for q-range data ≥ 0.04 Å^{-1}. For all samples, the intensity decay at high q follows a q^{-2} dependence. The insets to parts a and b are of I_0 versus C_s plots used to determine the C_{s0} for the S-20 and S-30 mixtures. A positive deviation of I_0 is observed for S-20 at 4 wt % while a negative deviation of I_0 is found for the 5 wt % S-30 samples.

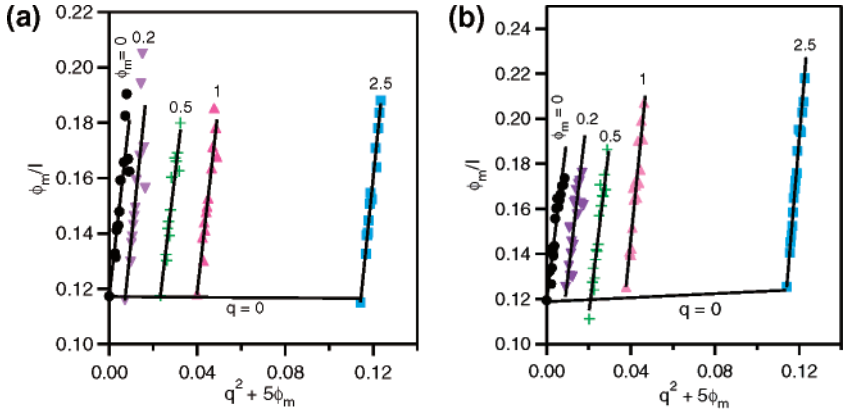

Figure 8. Zimm plots for (a) S-20 and (b) S-30 solutions at $0.2 \leq C_s \leq 2.5$ wt %.

observed, implying that to break up these clusters requires more enthalpic energy than entropic energy gained from the formation of dimers or monomers. One possibility may be that clusters are a more stable morphology for molecules having longer PEO groups (e.g., S-20 and S-30), because PEO is known to form large aggregates in aqueous solutions.[38,39] Moreover, the asymmetry of the two PEO chains, which is most likely larger for S-20 and S-30, is not well characterized, and may affect the molecular packing.[32] A detailed study on the effect of PEO asymmetry on aggregate morphologies is needed to conclusively resolve this issue.

Our time-dependent study of the 1 wt % S-10 sample seems to suggest that the pathway to cluster formation for samples with coexisting clusters/micelles may undergo a micellar phase because no clusters are observed within the first hour after sample preparation. Moreover, this transition has proved to be reversible (i.e., micelles → clusters) upon diluting the sample from ≥2 wt % to below 1 wt %.

Conclusion

Aqueous solutions of nonionic Gemini surfactants (S-10, S-20, and S-30) were studied using various techniques, SANS, DLS, and FS, to characterize their various morphologies. In contrast to the monomer → micelle (first cmc) and micelle → micelle (second cmc) transitions previously reported by Sato and Kishimoto,[21,22,24] the present work shows that S-10 does in fact undergo cluster/monomer → cluster/micelle → micelle transitions. The two critical surfactant concentrations corresponding to the above-mentioned transitions are consistent with the so-called "cmc" presented by Sato and Kishimoto.[21] Moreover, the cluster/monomer → micelle transition is similar to the vesicle → micelle transition observed in some other surfactant mixtures. To the best of our knowledge, the cluster/monomer → micelle transition has not been observed in any single-component surfactant solution. With time (~100 h), the clusters grow slowly in size, and their population density increases while in the cluster/micelle phase. Above 2 wt %, the cluster morphology is practically nonexistent. For S-20 samples, clusters and dimers/trimers coexist over the entire C_s regime studied (≤4 wt %). As for S-30 samples, large clusters are also observed for all samples studied and coexist with monomers up to 5 wt % without any micelle formation.

Acknowledgment. We benefited from many discussions with Kevin R. Lassila and Christine M. Kretz of Air Products and Chemicals, Inc. We would like to thank Paul C. DeRose (National Institute of Standards and Technology) for his help with the fluorescent spectroscopy experiments and SAMCOM funding from Air Products and Chemicals, Inc. We also thank Charles J. Glinka for SANS experiments on the degassed S-10 solution. This work utilized facilities supported in part by the National Science Foundation under Agreement No. DMR-9986442.

LA0494831

(38) Cuniberti, C. *Polymer* **1972**, *13*, 379−384; *Polymer* **1975**, *16*, 306−307.
(39) Layec, Y.; Layec-Raphalen, M. N. *J. Phys. Lett.* **1985**, *44*, 121−128.